Xiao et al. *NPG Asia Materials* (2022) 14:52
https://doi.org/10.1038/s41427-022-00399-z

NPG Asia Materials

ARTICLE Open Access

Sialylated glycan-modulated biomimetic ion nanochannels driven by carbohydrate–carbohydrate interactions

Jie Xiao[1,2], Wenqi Lu[2], Yahui Zhang[2], Minmin Li[2], Mingyang Li[2], Yuting Xiong[2], Mingliang Tang[3], Haijuan Qin[4], Zhichao Zhu[1] and Guangyan Qing[1,2]

Abstract

Ion channels play key roles in regulating the ion environment inside and outside the cell. Sialylated glycans (SGs) at the terminus of voltage-gated ion channels (VGICs) are abundant and directly control the switch of VGICs, while SGs on the cell surface are also closely related to virus infection, tumor growth, and metastasis. Here, we report a biomimetic ion nanochannel device that can be precisely regulated by SG. The nanochannel device is composed of a chemically etched polyethylene terephthalate film featuring conical nanochannels and a polyethyleneimine-*g*-malcopyranoside (abbreviated to Mal-PEI). Maltose, core-binding units in Mal-PEI, forms multiple hydrogen-bonding interactions with SG, which triggers globule-to-coil transition of the polymer chain and blocks transmembrane ion transport, resulting in a remarkable decrease in the ionic current of the nanochannel. Based on the changes in the ionic current, this device can precisely discriminate α2-3- and α2-6-linked sialyllactose, as well as SGs and neutral saccharides. Importantly, the nanochannel device can monitor the sialylation process of lactose catalyzed by α2,6-sialyltransferase in real time, showing its good potential in enzyme activity determination and in vitro enzyme identification. This work constructs an SG-modulated nanochannel with selective and smart ion-gating behavior, exhibiting unique advantages in SG responsiveness and enzymatic activity monitoring.

Introduction

The 2021 Nobel Prize in Physiology was awarded for discovering temperature and touch receptors, in which ion channels play vital roles in the conduction of electrical signals[1–3]. Controlling and regulating electrical signals are essential for normal physiological functions, including nerve activity, heartbeat, exercise process, and immune response. The initiation, conduction, and termination voltages of action potentials (AP) in cells originate from the active cooperation of various ion channels and transporters. Minor abnormalities in voltage-gated ion channels (VGICs) can lead to severe diseases, including arrhythmia, epilepsy, and paralysis. Many references have pointed out that these ion channel proteins could be modified with various N- and O-linked glycans with sialic acid as the terminal, which accounts for approximately 30% of the mass consisting of VGIC[4,5]. SG on the VGIC senses external stimuli and transmits information through electrostatic interactions to realize the regulation of the VGIC. Typical examples include $Na_V1.4$ sodium ion channels[6], $K_V1.1$ potassium ion channels[7], $Ca_V1.2$ calcium ion channels[8], and renal ion channels[9], which can all be regulated by SGs.

The most famous example is the infection of influenza A virus[8]. As illustrated in Scheme 1A, the influenza A virus first binds to α2-6-linked SG on the $Ca_V1.2$ ion channel, which opens VGIC and allows calcium ions to

Correspondence: Zhichao Zhu (zzcwuda@163.com) or Guangyan Qing (qinggy@dicp.ac.cn)
[1]College of Chemistry and Chemical Engineering, Wuhan Textile University, 1 Sunshine Road, Wuhan 430200, P. R. China
[2]Key Laboratory of Separation Science for Analytical Chemistry, Dalian Institute of Chemical Physics, Chinese Academy of Sciences, 457 Zhongshan Road, Dalian 116023, P. R. China
Full list of author information is available at the end of the article

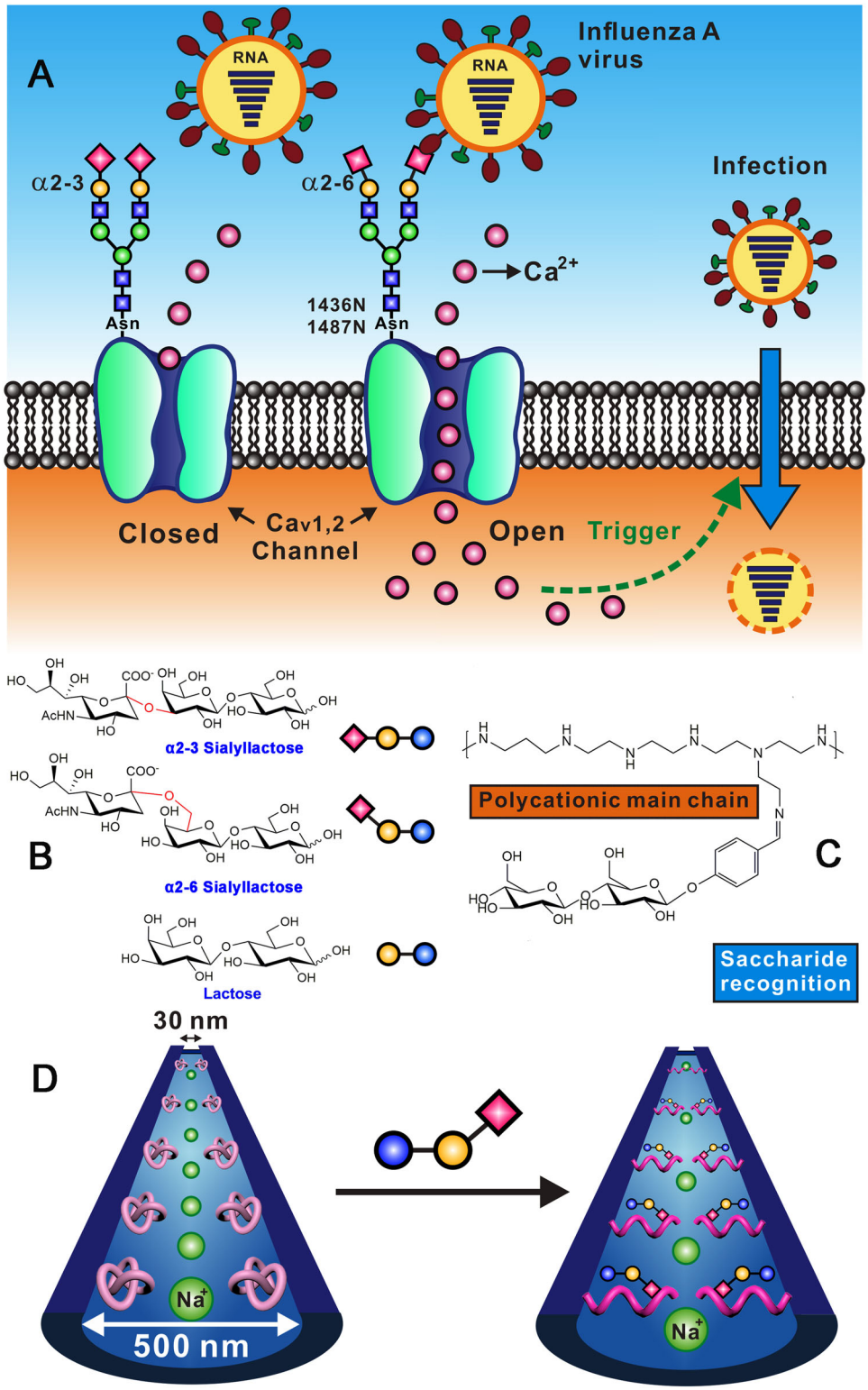

Scheme 1 **A** Schematic diagram of the infection process of influenza A virus entering the cell by first binding to α2-6-linked SG on voltage-dependent Ca^{2+} channel $Ca_V1.2$. **B** Chemical structures of α2-3/α2-6-linked sialyllactose and lactose. **C** Molecular design of a functional polymer capable of recognizing sialyllactose; maltose is grafted onto the polyethyleneimine main chain. **D** α2-6 sialyllactose-triggered globule-to-coil transition of the polymer chains immobilized on the inner surface of the conical nanochannel, which impacts ionic transport passing through the nanochannel.

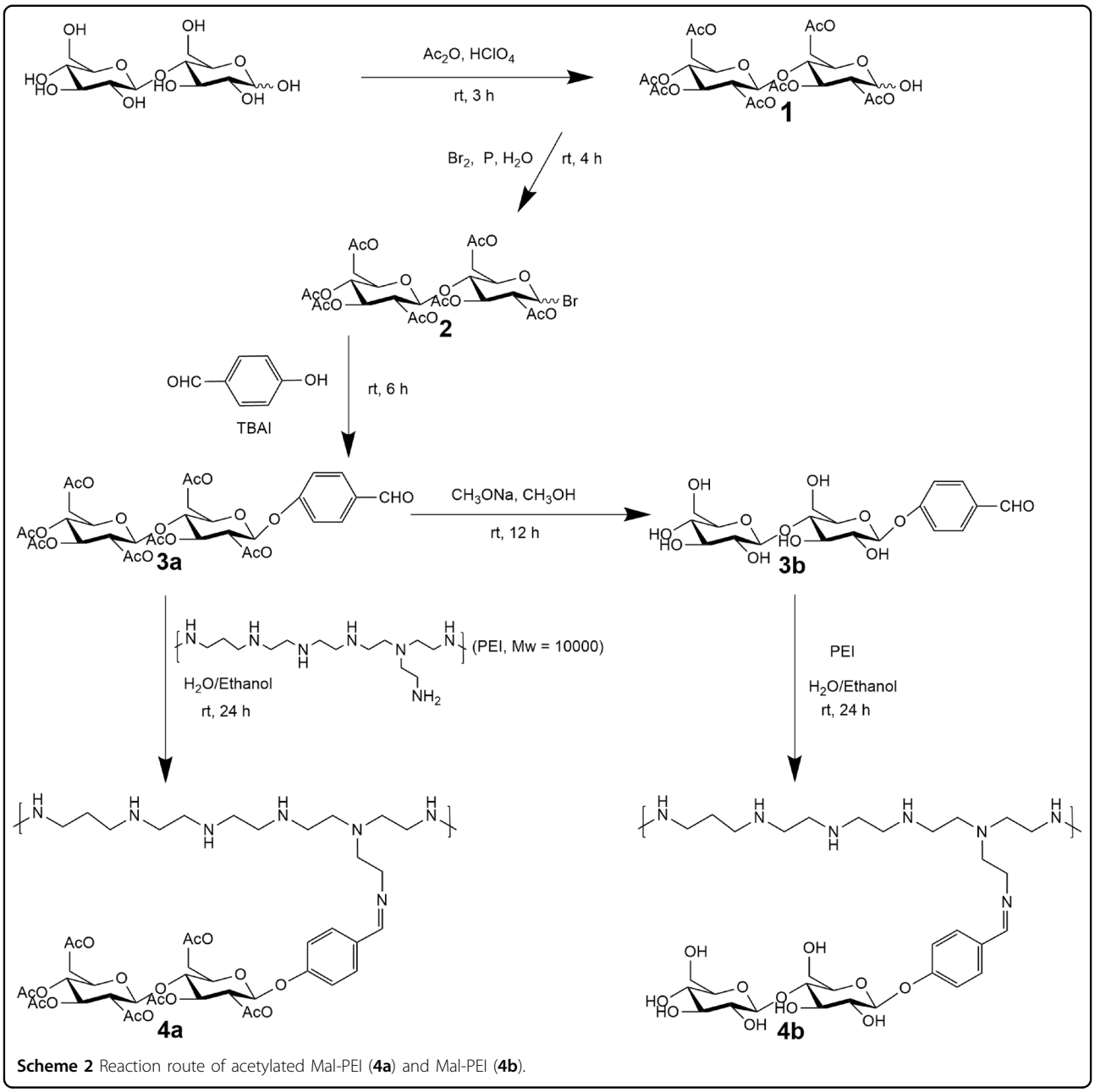

Scheme 2 Reaction route of acetylated Mal-PEI (**4a**) and Mal-PEI (**4b**).

enter the cell. The increase in the intracellular calcium ion concentration accelerates the endocytosis and absorption of the virus by the cell, which highlights the significance of SG in viral infection. From the perspective of glycochemistry, sialic acid usually binds adjacent monosaccharides *via* α-2,3- or α-2,6-linkages[10,11]. Different sialylated glycan linkage isomers can lead to completely different physiological effects. However, the structures of these linkage isomers are slightly different and difficult to distinguish. The main SG of the human upper respiratory tract is the α-2,6-linked type, and the hemagglutinin of influenza A H1N1 virus binds to this kind of SG. In contrast, the avian influenza subtype H5N1 binds to α-2,3-linked SG[12]. Therefore, H5N1 avian influenza has a poor ability to infect humans. In addition, the abnormal sialic acid expression on the cell surface is closely related to the occurrence of various cancers[13,14]. For example, prostate cancer is characterized by increased expression of α-2,3-linked SG, while lung cancer patients and breast cancer patients show overexpression of α-2,6-linked SG[15,16]. Recent research indicated that SG may also be related to the progression of Alzheimer's disease[17]. Therefore, accurately identifying various SGs and distinguishing and determining the connection types of the SG

chains are of great significance for the early diagnosis and targeted treatment of diseases.

On the other hand, inspired by the great significance of biological ion channels, various biomimetic ion nanochannels based on the electric field, ion potential, temperature, pH, and other stimulus-response modes have been developed in recent years, displaying excellent gating performance[18–22]. For example, Xie et al. modified nanochannels with azobenzene derivative-based polymers, and ionic transmission through the nanochannels could be adjusted by light and electric fields[23]. Sun et al. constructed a NO-regulated nanochannel based on a spiroring opening-closing reaction strategy[24]. Compared with artificial ion nanochannels regulated by various physical or small molecule stimuli, only a few works report biomimetic ion channels modulated by biomolecules, which are ubiquitous and play crucial roles in life processes. SG-modulated VGIC is a typical example; however, the development of glycan-specific affinity material and integration of the material with nanochannels are quite challenging.

Here, we report a biomimetic ion nanochannel regulated by SG based on a carbohydrate–carbohydrate interaction strategy. Different from conventional saccharide recognition design, such as lectin affinity, phenylboronic acid, oligopeptides, macrocyclic framework, and others[25–27], in this study, carbohydrate–carbohydrate interaction is introduced to recognize the SG. Maltose consists of two glucose units and has plentiful hydroxyls capable of forming multiple hydrogen-bonding interactions with the target glycan. Furthermore, maltose is grafted to a polyethyleneimine (PEI) chain through a five-step reaction, generating a glycan-affinity polymer (Mal-PEI, Scheme 2). Owing to the excellent ionic rectification effect, chemically etched polyethylene terephthalate (PET) film featuring conical nanochannels works as a substrate. Integration of Mal-PEI and PET film constructs an SG-sensitive nanochannel device. Selective binding between maltose and α2-6 sialyllactose initiates globule-to-coil transition of the polymer chain, which further determines the open and closed state of the nanochannel (Scheme 1D). Taking advantage of the sensitive changes in ionic current, sialyllactose linkage isomers, SG and neutral saccharides can be discriminated precisely. In addition, the nanochannel device can monitor the sialylation process of lactose catalyzed by sialyltransferases, showing the potential for real-time determination of enzyme activity.

Results and discussion

Characterization of PET conical nanochannels modified by a functional polymer

Because of the excellent rectification effect, PET conical nanochannel membranes were chosen as substrates[28] and were prepared using an asymmetric ion track-etching technique based on a customized electrochemical device (Fig. S6 in Supporting Information (SI))[29]. Scanning electron microscopy (SEM) observations indicated that the diameter of the base side of the nanopore was approximately 500 nm (Fig. 1C), while the diameter of the tip side of the nanopore was approximately 30 nm (Fig. 1D). Hydrogen nuclear magnetic resonance (^{1}H NMR, Fig. 1A, Fig. S4) and infrared (IR, Fig. S5) were used to verify the formation of the Mal-PEI polymer. According to the calculation of the peak area ratio in ^{1}H NMR, the grafting ratio of maltose on PEI was approximately 22%. Then, the Mal-PEI polymer was anchored to the inner wall of the PET conical nanochannels through a one-step coupling reaction (Fig. 1E). X-ray photoelectron spectroscopy (XPS) of the PET film before and after polymer modification indicated that the nitrogen (N) element content in the modified film significantly increased (Fig. 1F). Since the PET film itself did not contain N, the increase should be derived from the Mal-PEI polymer. In addition, the C1s (Fig. 1G), N1s (Fig. 1H), and O1s (Fig. 1I) core-level spectra of the polymer-modified PET film display the formation of C–N bonds and C=N bonds and an increase in the proportion of C–O bonds. These results confirmed the successful modification of the polymer on the PET film. Due to the hydrophilicity of maltose appended in the polymer, the static water contact angle (CA) of the PET film decreased from 75.7° to 65.2° after polymer modification (Fig. 1J, K). Then, the modified PET film was installed in a homemade electrochemical device, and a current–voltage test was performed. Figure 2A shows the current–voltage curves of the nanochannels before and after polymer modification. Because of the presence of abundant –COOH groups, the inner surface of the nanochannels was negatively charged. After polymer modification, a large number of amines in PEI were introduced, which endowed the inner surface with a positive charge. Therefore, a distinct upward current–voltage curve was observed, which further confirmed the successful grafting of the Mal-PEI polymer.

Transmembrane ionic current measurements

Then, the Mal-PEI-modified PET film was installed in the customized electrochemical device, and the transmembrane ionic current was recorded 10 min after the addition of a NaCl electrolyte containing different concentrations of saccharides. First, sialylated trisaccharides were chosen to perform the tests, namely, Neu5Ac-α2-3Galβ-1-4Glc (abbreviated to α2-3 sialyllactose) and Neu5Ac-α2-6Galβ-1-4Glc (abbreviated to α2-6 sialyllactose) sodium salts. A pair of model sialyllactose linkage isomers with similar composition to the SGs were found in the influenza A virus receptor. After adding α2-6 sialyllactose to the electrolyte, the current–voltage curves showed a remarkable change.

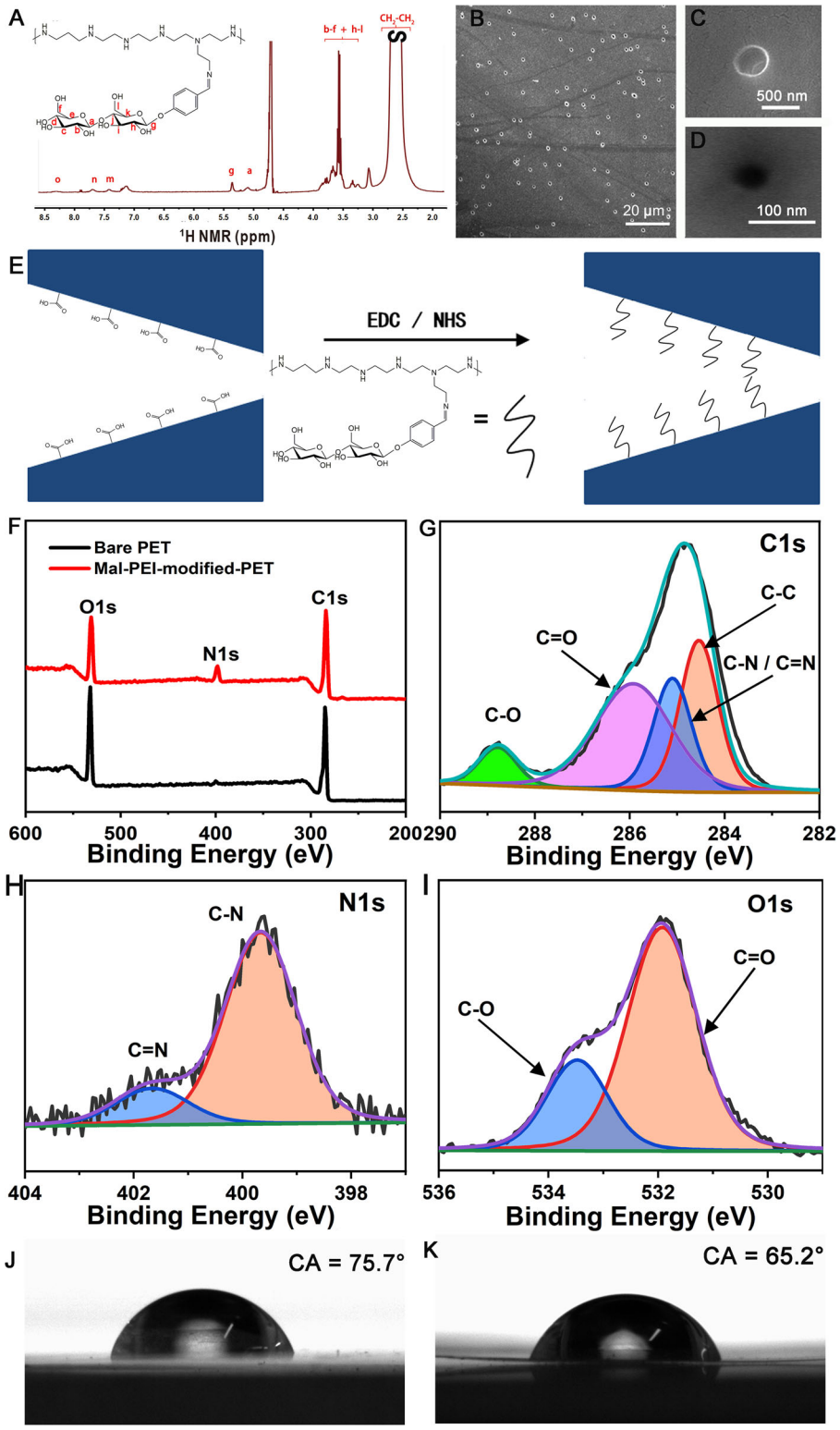

Fig. 1 Characterization of Mal-PEI-modified PET film with conical nanochannels. A ^{1}H NMR spectrum of Mal-PEI in D_2O at 25 °C. **B** Large-scale SEM image of an etched PET membrane featuring a large number of nanopores. **C**, **D** Amplified SEM images showing the morphology of the base side (**C**) and tip side **D** ends of the nanopore. **E** Grafting method of Mal-PEI onto the conical nanochannel. **F** XPS spectra of the etched PET film before (black) and after (red) the Mal-PEI modification. **G**–**I** C1s **G**, N1s **H**, and O1s **I** core-level spectra of the polymer-modified PET film. **J**, **K** Water droplet profiles displaying the surface water contact angle (CA) of the PET film before (**J**) and after **K** polymer modification.

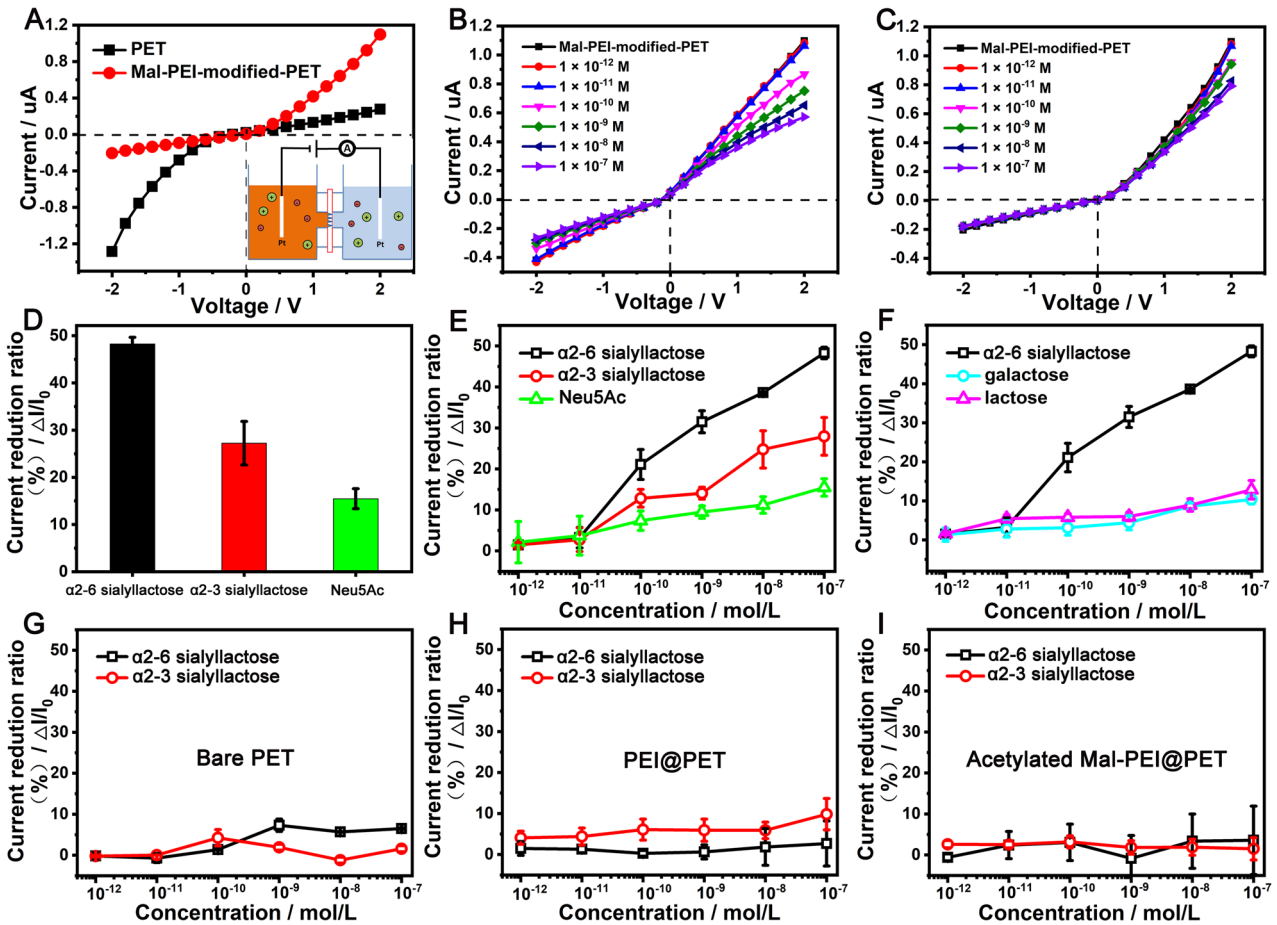

Fig. 2 Transmembrane ionic current tests. A Current–voltage curves of the etched PET film before (black) and after (red) Mal-PEI modification. **B**, **C** Current–voltage curves of Mal-PEI-modified PET film before and after additions of α2-6 (**B**) or α2-3 **C** sialyllactose solutions with different concentrations. **D** Comparison of the current reduction ratio of the films treated with α2-6 (black), α2-3 (red) sialyllactose and Neu5Ac (green) solutions (0.1 μM). **E**, **F** Concentration-dependent transmembrane ionic current decrease ratio ($\Delta I/I_0$) of the films upon treatment with α2-6, α2-3 sialyllactose, and Neu5Ac solutions (**E**) or α2-6 sialyllactose, galactose and lactose solutions **F**. **G**–**I** Concentration-dependent transmembrane ionic current decrease ratio ($\Delta I/I_0$) of bare PET film **G**, PEI-modified PET film (**H**), or acetylated Mal-PEI-modified PET film **I** treated with α2-6 (black) or α2-3 (red) sialyllactose solutions. All tests were conducted at 20 °C using 0.01 M NaCl solution as the electrolyte and repeated three times to obtain the average change ratios of the ionic current.

With the increase in the concentrations of α2-6 sialyllactose, the ionic current flowing through the nanochannels at +2 V decreased (Fig. 2B) from the initial 1.10 to 0.57 μA. With the increase in the concentration of α2-6 sialyllactose from 10^{-11} to 10^{-7} M, a linear relationship between the decrease in the current and the concentration of α2-6 sialyllactose could be built. The limit of detection (LOD) of the nanochannels for α2-6 sialyllactose was 0.59 pM, calculated through the formula LOD = 3*(SD/m)[30], where SD is the standard deviation of the blank signal and m is the slope of the calibration curve. The corresponding ionic current reduction ratio (defined as $[I–I_0]/I_0$) was 48% (the concentration of α2-6 sialyllactose was 0.1 μM, which was similar to that below), indicating that the functionalized nanochannels had a good response to α2-6 sialyllactose.

Under the same conditions, the response of the nanochannels to α2-3 sialyllactose was weaker. The final ionic current reduction ratio was 27% when 0.1 μM α2-3 sialyllactose was added (Fig. 2C). To determine a possible binding site in sialyllactose, Neu5Ac was evaluated as the terminal monosaccharide in the glycan. However, the final decrease rate in the ionic current was only 15% (Fig. 2D). Saccharide concentration-dependent ionic current variation further confirmed this difference (Fig. 2E), showing that the Mal-PEI-modified nanochannels had more remarkable responsiveness to α2-6 and α2-3 sialyllactose than Neu5Ac. This indicated that the Mal-PEI polymer

interacted with all SGs rather than the individual Neu5Ac unit.

Furthermore, lactose and galactose (the components of sialyllactose) were used to evaluate the responsiveness of the device. Twelve percent and 10% ionic current changes were detected for lactose and galactose (Fig. 2F), respectively, which confirmed the participation of these saccharide units in the complexation. Then, a series of control experiments were carried out. First, the bare PET conical nanochannel membranes were tested (Fig. 2G), and no evidential change in the current curve was detected for this pair of glycans. Then, the PET nanochannel membrane modified by the individual PEI was evaluated; similarly, neither α2-6 nor α2-3 sialyllactose induced an ionic current change (Fig. 2H), indicating that maltose in Mal-PEI was an indispensable binding molecule for the recognition of sialyllactose. There are abundant hydroxyls in maltose; thus, we assumed that multiple hydrogen bonding interactions between maltose and sialyllactose played a key role in the selective responsiveness of the device. To prove this assumption, acetylated protected maltose was grafted onto PEI (**4a** in Scheme 2), and the graft polymer was immobilized on the inner surface of the PET nanochannels. As shown in Fig. 2I, the acetylated Mal-PEI-modified nanochannels had no response to α2-6 or α2-3 sialyllactose, and this effect can be reasonably attributed to the largely weakened hydrogen bonding interactions induced by acetyl protection, highlighting the crucial role of carbohydrate–carbohydrate interactions. Two test solutions were prepared with maltose and α2-6 or α2-3 sialyllactose at a 2:1 molar ratio and added to the nanochannel device for competition assays (Fig. S7). The results showed that the nanochannel device showed no evidential change in response to the two mixed solutions. We presumed that the binding of free maltose with sialyllactoses blocked the recognition of sialyllactoses by the maltose on PEI immobilized on the inner surface of the nanochannel. The carbohydrate–carbohydrate interactions between maltose on the Mal-PEI polymer and sialyllactoses were confirmed.

Laser scanning confocal microscopy (LSCM) observation

To validate the binding events in the nanochannels, LSCM was used to observe the adsorption of α2-3 and α2-6 sialyllactoses onto the Mal-PEI-modified nanochannels. For the convenience of fluorescent tracing, both α2-3 and α2-6 sialyllactoses were labeled with fluorescein by an amination reaction at the reducing end of fluoresceinamine (Fig. 3A, B) in the presence of sodium cyanoborohydride. The crude products were purified by high-performance liquid chromatography (HPLC) on a C18 semipreparative column (Fig. 3C). The final product was confirmed by high-resolution mass spectrometry (Fig. 3D, HRMS). The Mal-PEI-modified PET film was immersed in an aqueous solution of fluorescein-labeled α2-3 or α2-6 sialyllactoses (10^{-7} M) for 10 min, and then the film was washed with water twice and dried under N_2 flows. Three-dimensional (3D) reconstructed LSCM images by layer-by-layer scanning recorded the morphology of the PET films. As shown in Fig. 3E, a large number of bright green cones were observed on the PET film upon treatment with the fluorescein-labeled α2-6 sialyllactose solution. After zooming in on the overall picture and observing the fluorescence picture of a single cone (right panel of Fig. 3E), the shape and pore size of a single cone were approximately consistent with those observed by SEM (Fig. S8), which can be attributed to the conical nanochannel. Both the Mal-PEI polymer and PET film are nonfluorescent, and the green fluorescent signals should originate from the adsorption of fluorescein-labeled α2-6 sialyllactose on the nanochannels. By comparison, when the film was treated with a fluorescein-labeled α2-3 sialyllactose solution, the observed green cones were not clear, and their fluorescent intensities were weaker, accompanied by evident background interference (Fig. 3F). From the perspective of 3D LCSM images, we presumed that α2-6 sialyllactose had a stronger adsorption capability on the nanochannel than α2-3 sialyllactose.

Adsorption dynamics on the polymer film

Mal-PEI was grafted onto the QCM resonator sensor surface to study the dynamic adsorption behavior of α2-3 or α2-6 sialyllactose on the polymer film by a quartz crystal microbalance with dissipation monitoring (QCM-D). The overall frequency shifts (ΔF) are dependent on the absorption quality of the analyte on the QCM sensor surface; the greater the mass of the analyte absorbed, the greater the degree of binding of the polymer toward the analyte[31]. As shown in Fig. 4A, upon injection of an α2-6 sialyllactose solution passing through the sensor, the ΔF value decreased gradually and reached equilibrium after 11 min, and the final ΔF value was approximately 34 Hz. By comparison, the α2-3 sialyllactose-induced ΔF variation was only 10 Hz, which was substantially smaller than that induced by α2-6 sialyllactose. The slow adsorption dynamics (~10 min) of α2-6 or α2-3 sialyllactose on the polymeric film also revealed that chemical adsorption rather than physical adsorption dominated the process; correspondingly, hydrogen bonding interactions between the Mal-PEI polymer and sialyllactose played a crucial role in the complexation and were superior to electrostatic adsorption. To confirm our speculation, pure PEI-modified sensors were also used to study the dynamic adsorption behavior by QCM-D. The adsorption process of pure PEI-modified sensors to two kinds of sialyllactoses was fast, and the amount of adsorption was small (Fig. S9). In this respect, the adsorption of sialyllactoses on sensors was physical adsorption caused by electrostatic interactions between sialyllactoses and PEI polymer. In addition,

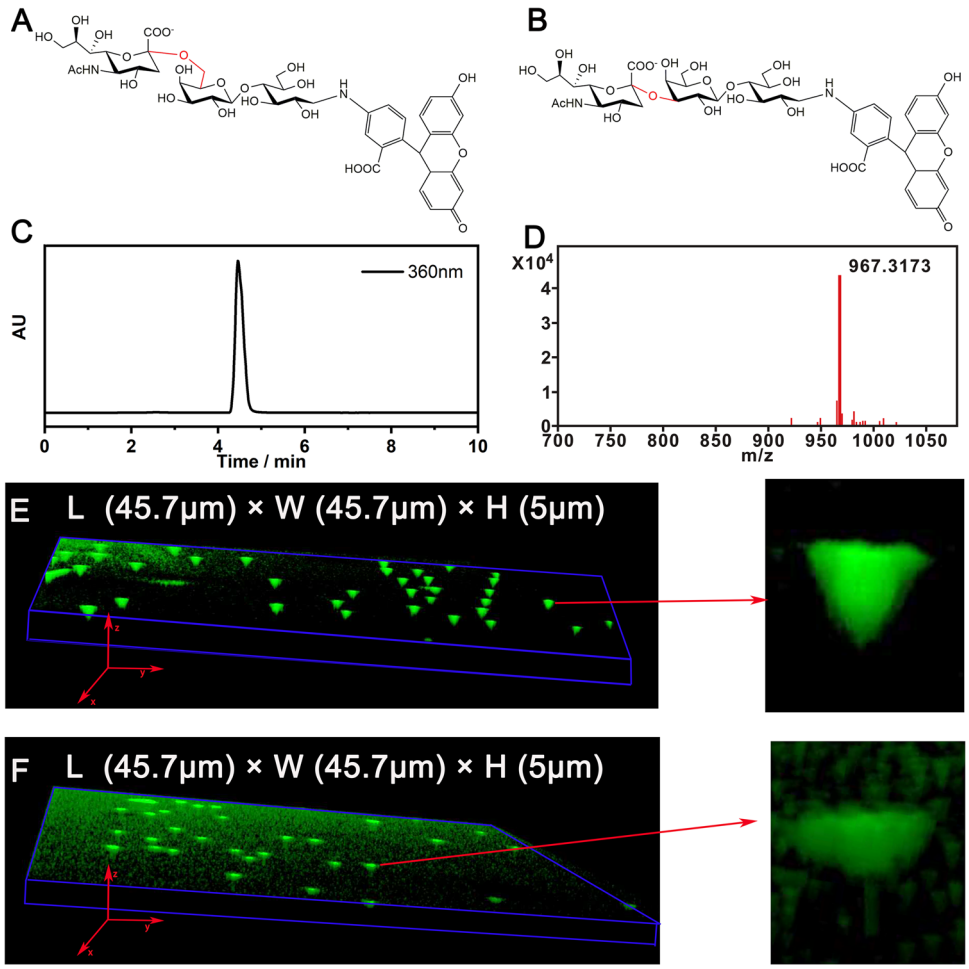

Fig. 3 Morphological observation of conical nanochannels by LSCM. A, **B** Chemical structures of fluorescein-labeled α2-6 (**A**) and α2-3 sialyllactose (**B**). **C**, **D** HPLC spectrum (**C**) for characterization of the purity of fluorescein-labeled α2-6 sialyllactose and its HRMS (**D**). **E**, **F** LSCM 3D images of the Mal-PEI-modified PET membrane treated with fluorescein-labeled α2-6 (**E**) or α2-3 (**F**) sialyllactose. The right panel shows the amplified morphology of a single conical nanochannel. Excitation wavelength: 465 nm.

the ΔF value difference caused by sialyllactoses was too small to be distinguished. These results further verified the critical role of carbohydrate–carbohydrate interactions in the response of the Mal-PEI polymer to sialyllactoses.

Moreover, QCM-D simultaneously provided an energy dissipation shift (ΔD), corresponding to the variation in conformation, thickness and viscoelasticity of the polymer. An upward curve often represents the swelling of the polymer film, whereas a downward curve represents the shrinkage behavior[32]. As shown in Fig. 4B, both α2-6 and α2-3 sialyllactoses displayed upward dissipation curves, revealing the remarkable swelling of the polymer film. ΔD induced by the adsorption of α2-6 sialyllactose (3.7×10^{-6}) was substantially larger than that induced by α2-3 sialyllactose (5×10^{-7}). QCM-D data clearly indicated that α2-6 sialyllactose had stronger adsorption on the Mal-PEI thin film than α2-3 sialyllactose, accompanied by more remarkable polymer swelling. Based on this knowledge, we presumed that the expansion of the polymer chain in response to sialyllactose adsorption might obstruct the conical nanochannels and that the smaller pore size of nanochannels would lead to a decrease in the transmembrane ionic current[33,34].

Atomic force microscopy (AFM)[35] was used to observe morphological changes in the Mal-PEI-modified QCM sensors before and after immersion in α2-3 or α2-6 sialyllactose solution (1 mM) for 10 min, respectively. As shown in Fig. 4C, D, remarkable variation in surface adhesion was detected when the sensor surface was treated with the α2-6 sialyllactose solution, and the average surface adhesion value increased from 12 nN to 24 nN (Fig. 4E). Moreover, the surface also became rougher, as detected from the height images (Fig. S10A, B). This result was consistent with the results recorded by the dissipation curves, both of which indicated that the

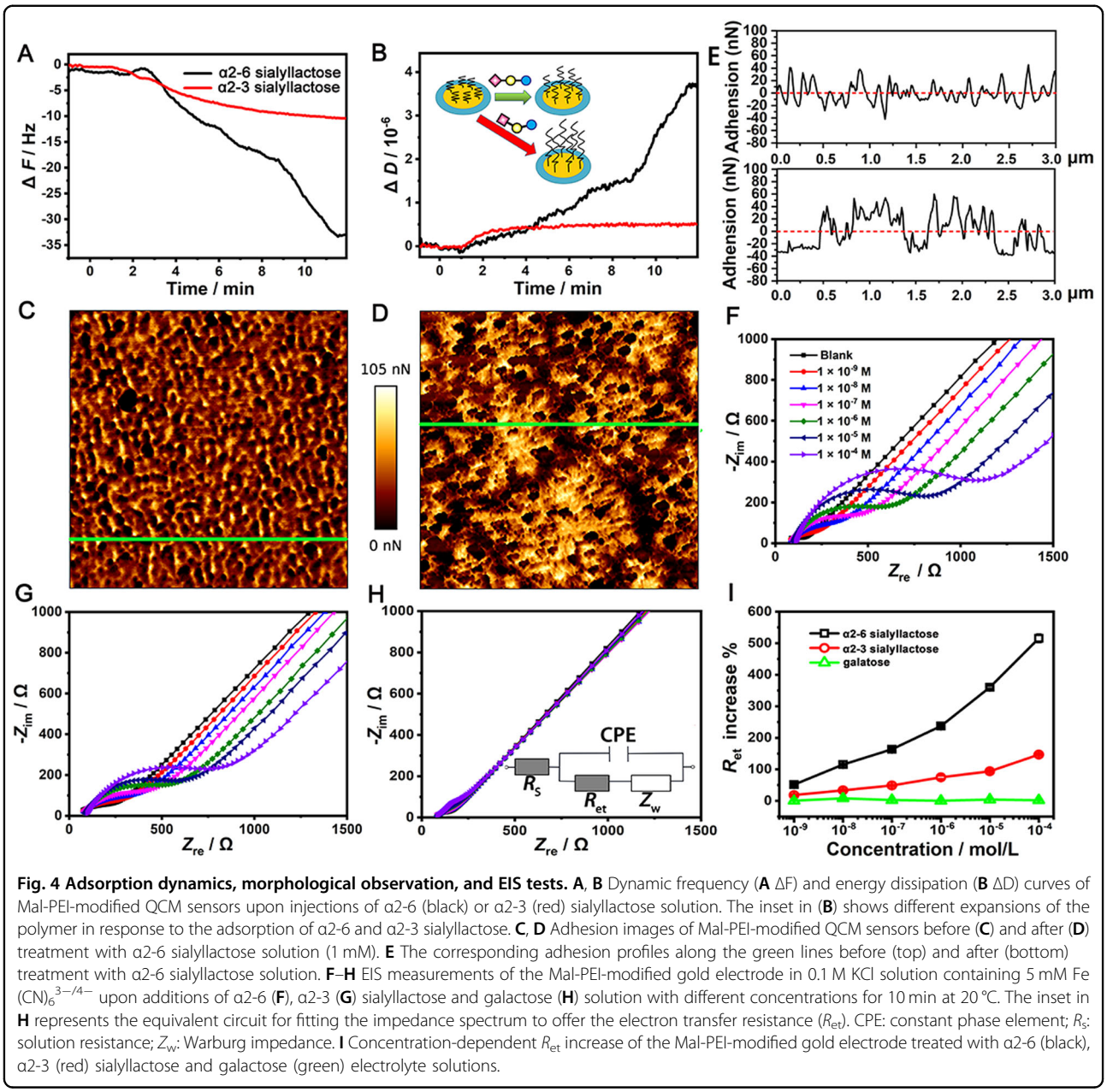

Fig. 4 Adsorption dynamics, morphological observation, and EIS tests. A, **B** Dynamic frequency (**A** ΔF) and energy dissipation (**B** ΔD) curves of Mal-PEI-modified QCM sensors upon injections of α2-6 (black) or α2-3 (red) sialyllactose solution. The inset in (**B**) shows different expansions of the polymer in response to the adsorption of α2-6 and α2-3 sialyllactose. **C**, **D** Adhesion images of Mal-PEI-modified QCM sensors before (**C**) and after (**D**) treatment with α2-6 sialyllactose solution (1 mM). **E** The corresponding adhesion profiles along the green lines before (top) and after (bottom) treatment with α2-6 sialyllactose solution. **F**–**H** EIS measurements of the Mal-PEI-modified gold electrode in 0.1 M KCl solution containing 5 mM Fe $(CN)_6^{3-/4-}$ upon additions of α2-6 (**F**), α2-3 (**G**) sialyllactose and galactose (**H**) solution with different concentrations for 10 min at 20 °C. The inset in **H** represents the equivalent circuit for fitting the impedance spectrum to offer the electron transfer resistance (R_{et}). CPE: constant phase element; R_S: solution resistance; Z_w: Warburg impedance. **I** Concentration-dependent R_{et} increase of the Mal-PEI-modified gold electrode treated with α2-6 (black), α2-3 (red) sialyllactose and galactose (green) electrolyte solutions.

polymer film became softer, corresponding to the expansion of the polymer chains. By comparison, no evidential change in adhesion and roughness was detected when the sensor surface was treated with α2-3 sialyllactose solution (Fig. S10C, D).

Conformational transition disclosed by electrochemical impedance spectroscopic (EIS) tests

The expansion of the polymer might influence the electrochemical process on the surface of the polymer, and this effect was investigated by EIS[36]. A gold electrode was modified with Mal-PEI through the same method as in QCM-D. The Mal-PEI-modified gold electrode was immersed in the saccharide electrolyte solution (5 mM Fe $(CN)_6^{3-/4-}$) for 10 min, and the EIS spectrum was recorded. Impedance spectra were plotted in the form of Nyquist plots (Fig. 4F–I) and fitted using an electronic equivalent circuit in order to derive the electron-transfer resistance (R_{et}) values by virtue of ZView software (version 2.1c, Fig. 4H inset). The semicircle diameter in the impedance spectra corresponds to R_{et} of the Mal-PEI layer[37]. After being immersed in a series of α2-6 sialyllactose solutions, the diameters of the semicircles grew gradually when the concentration of α2-6 sialyllactose increased, and

the calculated R_{et} value increased from the initial 157 Ω to 967 Ω when 10^{-4} M α2-6 sialyllactose was tested (Fig. 4F). The increase in the R_{et} value can be explained by the fact that the Mal-PEI polymer chains changed from an initially contracted state to an expanded state after interacting with α2-6 sialyllactose, which blocked the mass transport of $Fe(CN)_6^{3-/4-}$ from the bulk solution to the surface of the electrode through the polymer film.

Compared with α2-6 sialyllactose, the increase in semicircle diameter in the impedance spectra of α2-3 sialyllactose was smaller (Fig. 4G), which indicated that the degree of expansion caused by α2-3 sialyllactose was less than that caused by α2-6 sialyllactose. Galactose is a neutral monosaccharide that exists in these two sialyllactoses, and an EIS test of galactose was also carried out. No evidential change was detected in the impedance spectra (Fig. 4H), which revealed that galactose had a weak influence on the polymer conformation. This in turn highlights the importance of the sialic acid unit. Concentration-dependent R_{et} increase curves further validated the remarkable difference among α2-6, α2-3 sialyllactose and galactose (Fig. 4I) when they interacted with the polymers. Furthermore, the pure PEI-modified gold electrode was also tested by EIS. Neither α2-6 nor α2-3 sialyllactose produced an evidential response in Nyquist plots (Fig. S11). Therefore, the recognition of sialyllactoses by the Mal-PEI polymer can be reasonably attributed to the carbohydrate–carbohydrate interactions between maltose and sialyllactoses.

Dynamic Light Scattering (DLS) Tests

The swelling of the polymer chains was revealed by DLS tests in solution[38]. The average particle size of Mal-PEI in H_2O (1 mg mL^{-1}) was measured to be 10.3 nm (Fig. 5A). After mixing with α2-3 or α2-6 sialyllactose, the average particle size of the polymer increased to 20.5 nm (Fig. 5B) or 29.1 nm (Fig. 5C), respectively. Therefore, the DLS test provided solid evidence for the expansion of the polymer chain.

Binding affinity analysis

Isothermal titration microcalorimetry (ITC) experiments were performed to measure the binding affinity (K_a) of the polymer with sialyllactoses in solution[39]. α2-6 or α2-3 sialyllactoses solution was dropped into the Mal-PEI solution, and the exothermic value was recorded (Fig. 5D). According to a series of exothermic amounts, K_a could be obtained by nonlinear fitting (Fig. 5E). The K_a of the polymer with α2-6 sialyllactose was 3.05×10^5 M^{-1}, which was larger than that with α2-3 sialyllactose (2.18×10^5 M^{-1}, Fig. 5F). The ITC result was consistent with the previous data collected in LSCM and QCM-D, which all proved that Mal-PEI had stronger binding affinity with α2-6 sialyllactose than with α2-3 sialyllactose.

Carbohydrate–carbohydrate interactions between maltose and sialyllactose

The transmembrane ionic current tests (Fig. 2H, I) indicated that maltose played crucial role in the complexation between Mal-PEI and sialyllactose. ITC experiments revealed that the K_a of maltose and α2-6 sialyllactose was approximately 5.10×10^5 M^{-1} based on a 1:1 binding mode, while the K_a of maltose and α2-3 sialyllactose was 2.97×10^5 M^{-1} (Fig. S12). A clear difference in K_a indicated that maltose had different interactions with α2-6 and α2-3 sialyllactose, which endowed Mal-PEI with the capacity to distinguish α2-3 from α2-6 sialyllactose. An additional ITC test indicated that maltose also had moderate affinity with galactose (K_a: 2.41×10^4 M^{-1}), which provided extra binding sites with the glycans.

The binding details between maltose and α2-6 sialyllactose or α2-3 sialyllactose were investigated by ^1H NMR spectra. Figure 6A shows the number of each hydrogen proton in maltose and sialyllactoses. When maltose interacted with equimolar α2-6 sialyllactose (Fig. 6B–D), remarkable changes were detected. For example, the ^{d}OH2 and ^{e}OH2 protons in maltose displayed downfield shifts, and the multiplet peaks converged into broad peaks, as indicated by the blue regions. ^{b}OH2-4, ^{c}OH2,4,6, and ^{a}OH7-9 in α2-6 sialyllactose also exhibited a downfield shift, revealing intensive multiple hydrogen bonding interactions between maltose and α2-6 sialyllactose. Similar chemical shift changes were also observed when maltose interacted with α2-3sialyllactose (Fig. 6E–G), but the variations in the ^{d}OH2 and ^{e}OH2 protons in maltose were smaller. From the comparison of the partial ^1H-^1H COSY spectrum of 2-6 sialyllactose, 2-3 sialyllactose, maltose, and their mixtures, it could also be concluded that maltose has a stronger binding ability to 2-6 sialyllactose than to 2-3 sialyllactose (Fig. S13).

In addition, possible binding models between maltose and α2-6 or α2-3 sialyllactose were obtained through quantum chemistry based on the Gaussian 09 software package. Figure 6H shows the interaction model of maltose with α2-6 sialyllactose. Five sets of intermolecular hydrogen bonds formed, and the lengths were 1.69, 2.38, 1.62, 1.65, and 1.66 Å, respectively. The short bond lengths corresponded to the strong complexation. By comparison, six sets of intermolecular hydrogen bonds with lengths of 1.88, 2.12, 2.06, 2.40, 3.06, and 2.48 Å formed between maltose and α2-3 sialyllactose (Fig. 6I), and the longer bond lengths indicated that the complexation of maltose with α2-3 sialyllactose was weaker than that with α2-6 sialyllactose. It is worth noting that the binding models shown here are only two possible models. Considering the complexity of carbohydrate–carbohydrate interactions, a more detailed structural analysis should be performed in the future.

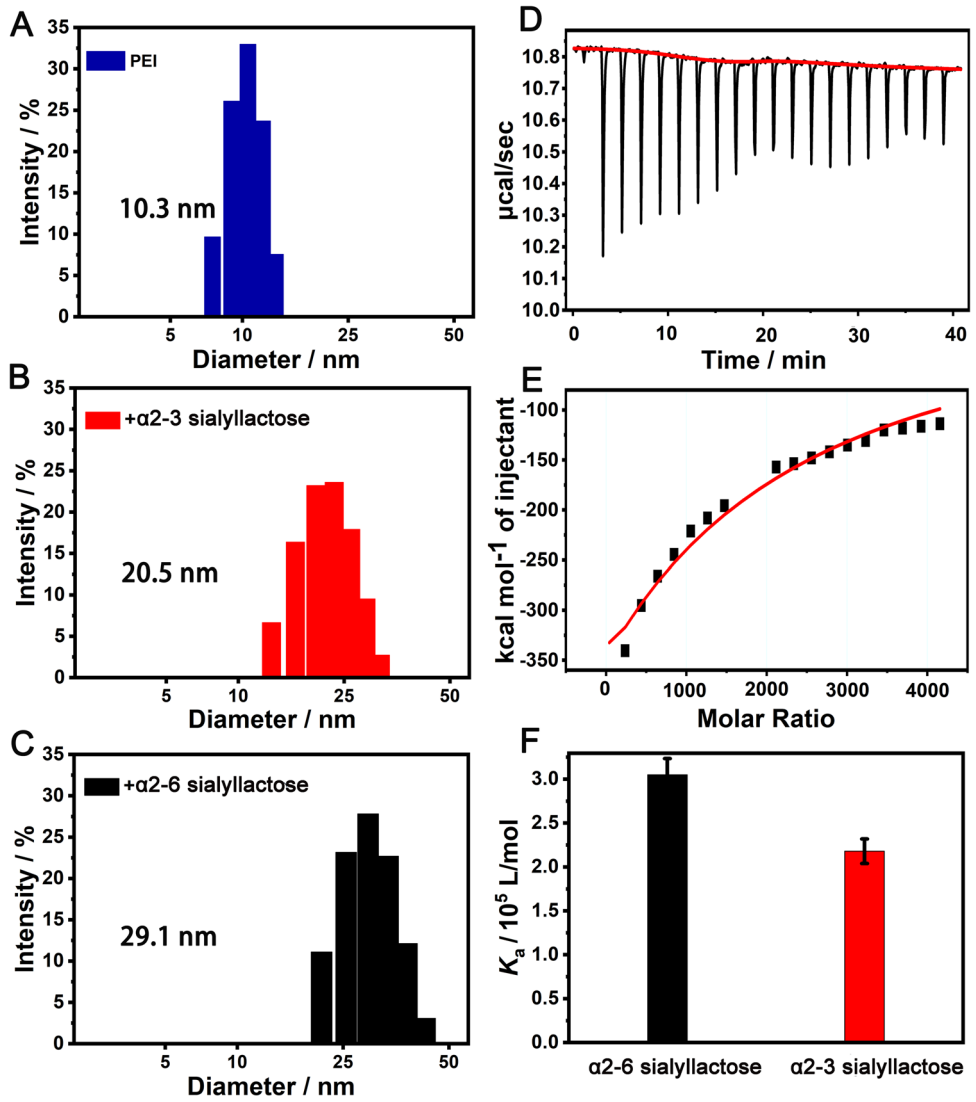

Fig. 5 DLS tests and binding affinity analysis. A–C Hydrodynamic diameter distribution of the Mal-PEI polymer (1 mg mL^{-1}) before (**A**) and after additions of 10^{-6} M α2-3 (**B**) and α2-6 (**C**) sialyllactose in H_2O, determined by DLS. **D** ITC data recorded for titration of Mal-PEI solution (0.08 mg·mL^{-1}) with additions of different equivalents of α2-6 sialyllactose. **E** Nonlinear fitting curve of Mal-PEI interacting with α2-6 sialyllactose using a sequential binding site model to calculate binding affinity (K_a). **F** Comparison of K_a values of Mal-PEI with α2-6 (black) and α2-3 (red) sialyllactose.

Possible explanation for conformational transition of the polymer

Based on the experimental results and interaction models proposed above, a potential conformational change mechanism is proposed to explain the effect observed in the nanochannels. Initially, maltose interacts with neighboring maltose molecules or the secondary amines in PEI through hydrogen bonding interactions, which results in a contracted conformation of the polymeric chain (central panel in Fig. 6J). Strong binding between maltose and α2-6 sialyllactose destroys the initial polymer network, promoting the transition of the polymeric chains from the contracted state to a swollen state (left panel in Fig. 6J). By comparison, the interaction of maltose with α2-3 sialyllactose is weaker than that with α2-6 sialyllactose, and only part of the initial polymer network is broken; thus, the polymeric chains exhibit slight swelling (right panel in Fig. 6J). Remarkable expansion of the polymeric film decreases the diameters of the nanochannels, which blocks transmembrane ionic transport and reduces the ionic current. The Mal-PEI polymers have different binding affinities with α2-6 and α2-3 sialyllactoses. Therefore, the binding-induced expansion degrees of the polymeric chains are different, which is reflected in different variations in the ionic current.

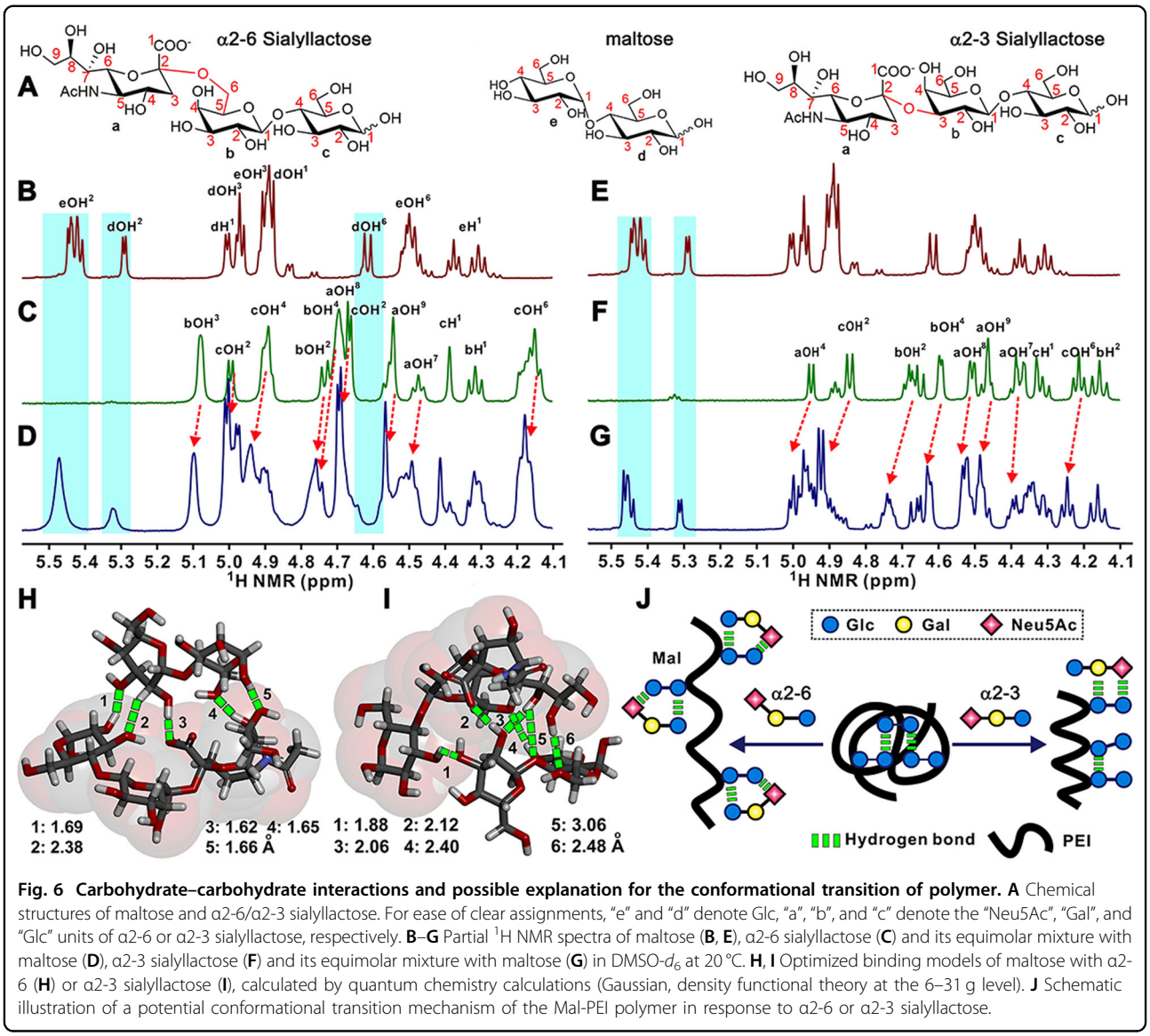

Fig. 6 Carbohydrate–carbohydrate interactions and possible explanation for the conformational transition of polymer. A Chemical structures of maltose and α2-6/α2-3 sialyllactose. For ease of clear assignments, "e" and "d" denote Glc, "a", "b", and "c" denote the "Neu5Ac", "Gal", and "Glc" units of α2-6 or α2-3 sialyllactose, respectively. **B**–**G** Partial ^{1}H NMR spectra of maltose (**B**, **E**), α2-6 sialyllactose (**C**) and its equimolar mixture with maltose (**D**), α2-3 sialyllactose (**F**) and its equimolar mixture with maltose (**G**) in DMSO-d_6 at 20 °C. **H**, **I** Optimized binding models of maltose with α2-6 (**H**) or α2-3 sialyllactose (**I**), calculated by quantum chemistry calculations (Gaussian, density functional theory at the 6–31 g level). **J** Schematic illustration of a potential conformational transition mechanism of the Mal-PEI polymer in response to α2-6 or α2-3 sialyllactose.

Monitoring of enzymatic reactions

Sialyltransferases are a family of glycosyltransferases that play an integral role in the biosynthesis of Neu5Ac-containing oligosaccharides and glycoconjugates, which are closely related to the occurrence of cancers. To display the application of Mal-PEI nanochannels in monitoring enzymatic sialylation reactions, α2,6-sialyltransferase was introduced to catalyze the transfer of Neu5Ac from cytidine 5′-monophosphate-N-acetylneuraminic acid (CMP-NeuAc) to a lactose substrate[40]. Briefly, lactose (0.1 μM) and CMP-Neu5Ac (150 μM) were prepared based on a buffer solution (100 mM Tris-HCl, pH 7.5). Then, 2 mL lactose solution and 20 μL CMP-Neu5Ac were injected into the current measurement apparatus mounted with a piece of Mal-PEI-modified nanochannel membrane, and the temperature of the entire apparatus was maintained at ~37 °C. Then, α2,6-sialyltransferase (5 mU) was added to activate the enzymatic reaction (Fig. 7A, top), while the ionic current was continuously recorded. The recorded ionic current value (at +2 V) decreased with the extension of reaction time (Fig. 7B), from 0.29 μA at the beginning to 0.19 μA at 16 min (Fig. 7C). HRMS data further confirmed the formation of α2-6 sialyllactose (Fig. 7A, bottom) in the resulting product mixture. This test was repeated three times with three pieces of Mal-PEI-modified nanochannel membrane. As shown in Fig. 7D, the obtained mean current values along with the standard deviation were plotted versus the reaction time. The current reduction ratio reached a maximum value of approximately 32% at 16 min.

Furthermore, the sialylation processes of trisaccharide (i.e., 2′-fucosyllactose, Fig. S14) and glycopeptide

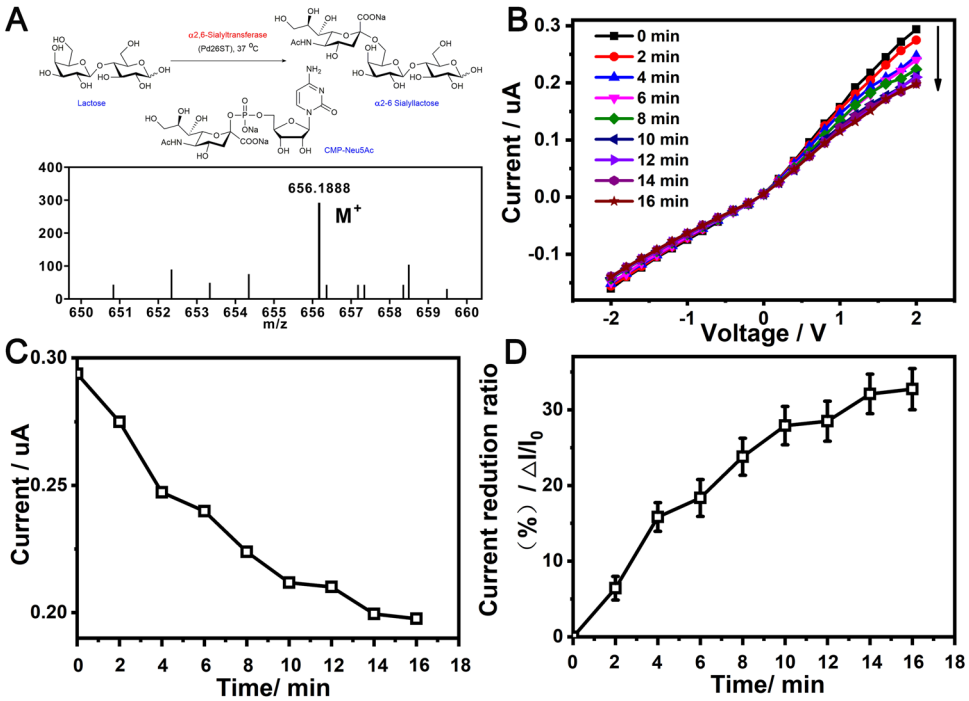

Fig. 7 Monitoring of enzymatic reactions. A Enzymatic sialylation reaction scheme of CMP-Neu5Ac with lactose (top) catalyzed by α2,6-sialyltransferase and HRMS of the product α2-6 sialyllactose (bottom). **B** Time-dependent current–voltage curves of Mal-PEI-modified PET nanochannels for the enzymatic sialylation reaction. **C** Time-dependent current at +2 V. **D** Time-dependent transmembrane ionic current decrease ratio (at +2 V). Error bars represent the standard deviations obtained from three ionic current measurements.

(obtained from tryptic digests of IgG, Fig. S15A,B) were monitored. The recorded ionic current value (at +2 V) decreased with the extension of reaction time, and current reduction ratios were approximately 26 and 15% at 16 min for 2′-fucosyllactose and tryptic digests of IgG, respectively. These results revealed the good potential of nanochannel devices for monitoring enzymatic sialylation reactions in real time. It is worth pointing out that the sialylation process of glycoprotein (IgG as an example, Fig. S15C) was difficult to monitor due to the more complex structure and the hidden glycosylation sites of glycoprotein.

Conclusions

Inspired by the SG-regulated VGIC that plays crucial role in influenza A virus infection, we developed a biomimetic ion nanochannel device that had sensitive and selective responsiveness to α2-6-linked sialyllactose, which further realizes the "ON–OFF" ion flux change of the nanochannel. Compared with conventional nanochannel devices modulated by physical or small molecule stimulation, the development of glycan-regulated nanochannels is more challenging due to the complicated composition and structure of glycans. This work indicated that a glycan recognition system and corresponding nanochannel device could be constructed through smart polymer design, and the remarkable globule-to-coil transition of the polymer chain driven by carbohydrate–carbohydrate interactions paved a new route for the future development of glycan-responsive biochips and biodevices. Our future planned work focuses on optimizing functionalized nanochannels and combining functional polymers with a single nanochannel for the single-molecule analysis of glycans. The present study displays the good potential of the nanochannel device in monitoring enzymatic sialylation reactions. This real-time monitoring method avoids the use of high-cost antibodies and complex pretreatment processes, which may promote the development of inhibitor target SGs.

Acknowledgements

This work was supported by the National Natural Science Foundation of China (21775116, 21922411, 22004120, and 22104013), DICP Innovation Funding (DICP-RC201801, I202008), LiaoNing Revitalization Talents Program (XLYC1802109) and Dalian Outstanding Young Scientific Talent (2020RJ01).

Author details

[1]College of Chemistry and Chemical Engineering, Wuhan Textile University, 1 Sunshine Road, Wuhan 430200, P. R. China. [2]Key Laboratory of Separation Science for Analytical Chemistry, Dalian Institute of Chemical Physics, Chinese Academy of Sciences, 457 Zhongshan Road, Dalian 116023, P. R. China. [3]College of Life Sciences, Wuhan University, Wuhan 430072, P. R. China. [4]Research Centre of Modern Analytical Technology, Tianjin University of Science and Technology, Tianjin 300457, P. R. China

Author contributions

G.Q. conceived the idea. J.X. W.L., and Y.Z. fabricated the samples and performed the experiments. M.M.L. M.Y.L., and Y.X. helped to analyze the experimental data. M.T. performed the LSCM measurements. H.Q. collected the NMR data. Z.Z. and G.Q. supervised this study. All authors contributed to writing and editing the article.

Conflict of interest

The authors declare no competing interests.

Publisher's note

Springer Nature remains neutral with regard to jurisdictional claims in published maps and institutional affiliations.

Supplementary information The online version contains supplementary material available at https://doi.org/10.1038/s41427-022-00399-z.

Received: 5 January 2022 Revised: 8 May 2022 Accepted: 10 May 2022.
Published online: 17 June 2022

References

1. Bautista, D. M. et al. The menthol receptor TRPM8 is the principal detector of environmental cold. *Nature* **448**, 204–208 (2007).
2. Coste, B. et al. Piezo1 and Piezo2 are essential components of distinct mechanically activated cation channels. *Science* **330**, 55–60 (2010).
3. Kefauver, J. M., Ward, A. B. & Patapoutian, A. Discoveries in structure and physiology of mechanically activated ion channels. *Nature* **587**, 567–576 (2020).
4. Liu, Z., Tao, J., Ye, P. & Ji, Y. Mining the virgin land of neurotoxicology: a novel paradigm of neurotoxic peptides action on glycosylated voltage-gated sodium channels. *J. Toxicol.* **2012**, 843787 (2012).
5. Jiang, H. et al. Modulating cell-surface receptor signaling and ion channel functions by in situ glycan editing. *Angew. Chem. Int. Ed.* **57**, 967–971 (2018).
6. Bennett, E. S. Isoform-specific effects of sialic acid on voltage-dependent Na^+ channel gating: functional sialic acids are localized to the S5-S6 loop of domain i. *J. Physiol.* **538**, 675–690 (2002).
7. Cartwright, T. A. & Schwalbe, R. A. Atypical sialylated N-glycan structures are attached to neuronal voltage-gated potassium channels. *Biosci. Rep.* **29**, 301–313 (2009).
8. Fujioka, Y. et al. A sialylated voltage-dependent Ca^{2+} channel binds hemagglutinin and mediates influenza a virus entry into mammalian cells. *Cell Host Microbe* **23**, 809–818 (2018).
9. Cha, S.-K. et al. Removal of sialic acid involving Klotho causes cell-surface retention of TRPV5 channel *via* binding to galectin-1. *Proc. Natl Acad. Sci. USA* **105**, 9805–9810 (2008).
10. Reily, C., Stewart, T. J., Renfrow, M. B. & Novak, J. Glycosylation in health and disease. *Nat. Rev. Nephrol.* **15**, 346–366 (2019).
11. Chen, S., Qin, R. & Mahal, L. K. Sweet systems: Technologies for glycomic analysis and their integration into systems biology. *Crit. Rev. Biochem. Mol. Biol.* **56**, 301–320 (2021).
12. Kumlin, U., Olofsson, S., Dimock, K. & Arnberg, N. Sialic acid tissue distribution and influenza virus tropism. *Influenza Other Respir. Viruses* **2**, 147–154 (2008).
13. Schultz, M. J., Swindall, A. F. & Bellis, S. L. Regulation of the metastatic cell phenotype by sialylated glycans. *Cancer Metastasis Rev.* **31**, 501–518 (2012).
14. Bull, C., Stoel, M. A., den Brok, M. H. & Adema, G. J. Sialic acids sweeten a tumor's life. *Cancer Res.* **74**, 3199–3204 (2014).
15. Kim, Y. J. & Varki, A. Perspectives on the significance of altered glycosylation of glycoproteins in cancer. *Glycoconj. J.* **14**, 569–576 (1997).
16. Cha, S.-K. et al. Global cancer statistics 2018: GLOBOCAN estimates of incidence and mortality worldwide for 36 cancers in 185 countries. *Ca-Cancer J. Clin.* **68**, 394–424 (2018).
17. Liu, D. et al. O-glycosylation induces amyloid-β to form new fibril polymorphs vulnerable for degradation. *J. Am. Chem. Soc.* **142**, 20216–20223 (2021).
18. Han, C. et al. Enantioselective recognition in biomimetic single artificial nanochannels. *J. Am. Chem. Soc.* **133**, 7644–7647 (2011).
19. Li, C.-Y. et al. Solution-pH-modulated rectification of ionic current in highly ordered nanochannel arrays patterned with chemical functional groups at designed positions. *Adv. Funct. Mater.* **23**, 3836–3844 (2013).
20. Wang, R. et al. Temperature-sensitive artificial channels through pillar[5]arene-based host-guest interactions. *Angew. Chem. Int. Ed.* **56**, 5294–5298 (2017).
21. Liao, Q.-L. et al. A single nanowire sensor for intracellular glucose detection. *Nanoscale* **11**, 10702–10708 (2019).
22. de la Escosura-Muniz, A. & Merkoci, A. Nanochannels preparation and application in biosensing. *ACS Nano* **6**, 7556–7583 (2012).
23. Xie, G. et al. Light- and electric-field-controlled wetting behavior in nanochannels for regulating nanoconfined mass transport. *J. Am. Chem. Soc.* **140**, 4552–4559 (2018).
24. Sun, Y. et al. A highly selective and recyclable NO-responsive nanochannel based on a spiroring opening-closing reaction strategy. *Nat. Commun.* **10**, 1323 (2019).
25. Zielinska, D. F., Gnad, F., Wisniewski, J. R. & Mann, M. Precision mapping of an in vivo N-glycoproteome reveals rigid topological and sequence constraints. *Cell* **141**, 897–907 (2010).
26. Zhang, W., Peng, B., Tian, F., Qin, W. & Qian, X. Facile preparation of well-defined hydrophilic core-shell upconversion nanoparticles for selective cell membrane glycan labeling and cancer cell imaging. *Anal. Chem.* **86**, 482–489 (2014).
27. Qiao, J., Song, Y., Chen, C. & Qi, L. In situ determination of sialic acid on cell surface with a pH-regulated polymer enzyme nanoreactor. *Anal. Chem.* **93**, 7317–7322 (2021).
28. Ding, D., Gao, P., Ma, Q., Wang, D. & Xia, F. Biomolecule-functionalized solid-state ion nanochannels/nanopores: features and techniques. *Small* **15**, 1804878 (2019).
29. Fang, R. et al. Supramolecular self-assembly induced adjustable multiple gating states of nanofluidic diodes. *J. Am. Chem. Soc.* **138**, 16372–16379 (2016).
30. Ganesana, M., Trikantzopoulos, E., Maniar, Y., Lee, S. T. & Venton, B. J. Development of a novel micro biosensor for in vivo monitoring of glutamate release in the brain. *Biosens. Bioelectron.* **130**, 103–109 (2019).
31. Cho, N.-J., Frank, C. W., Kasemo, B. & Hook, F. Quartz crystal microbalance with dissipation monitoring of supported lipid bilayers on various substrates. *Nat. Protoc.* **5**, 1096–1106 (2010).
32. Olsson, A. L. J., Quevedo, I. R., He, D., Basnet, M. & Tufenkji, N. Using the quartz crystal microbalance with dissipation monitoring to evaluate the size of nanoparticles deposited on surfaces. *ACS Nano* **7**, 7833–7843 (2013).
33. Long, Z. et al. Recent advances in solid nanopore/channel analysis. *Anal. Chem.* **90**, 577–588 (2018).
34. Ai, M. et al. Ionic transport through chemically functionalized hydrogen peroxide-sensitive asymmetric nanopores. *ACS Appl. Mater. Interfaces* **7**, 19541–19545 (2015).
35. Butt, H. J., Cappella, B. & Kappl, M. Force measurements with the atomic force microscope: Technique, interpretation and applications. *Surf. Sci. Rep.* **59**, 1–152 (2005).
36. Zhou, F. et al. Probing the responsive behavior of polyelectrolyte brushes using electrochemical impedance spectroscopy. *Anal. Chem.* **79**, 176–182 (2007).
37. Ding, S., Cao, S., Zhu, A. & Shi, G. Wettability switching of electrode for signal amplification: conversion of conformational change of stimuli-responsive polymer into enhanced electrochemical chiral analysis. *Anal. Chem.* **88**, 12219–12226 (2016).
38. Bhattacharjee, S. DLS and zeta potential - What they are and what they are not? *J. Controlled Release* **235**, 337–351 (2016).
39. Linkuviene, V., Krainer, G., Chen, W.-Y. & Matulis, D. Isothermal titration calorimetry for drug design: precision of the enthalpy and binding constant measurements and comparison of the instruments. *Anal. Biochem.* **515**, 61–64 (2016).
40. Xu, Y. et al. Successfully engineering a bacterial sialyltransferase for regioselective alpha 2,6-sialylation. *ACS Catal.* **8**, 7222–7227 (2018).